Proceedings of the 21st ICSMGE, Vienna, Austria, 14 – 19 June 2026. Pistrol, Adam & Schweiger (eds.)
Published by: ÖGG, Austrian Society for Geomechanics, Salzburg, Austria, ISBN 978-3-9503898-4-5
https://doi.org/10.53243/ICSMGE2026-1086

Experimental study of hybrid seabed anchors: anchor geometry, installation and pullout under inclined loading

Yuqi Mi
School of Civil and Environmental Engineering, Georgia Institute of Technology, Atlanta, USA, ymi36@gatech.edu

Fernando Patino-Ramirez
School of Civil and Environmental Engineering, Georgia Institute of Technology, Atlanta, USA; Department of Civil and Environmental Engineering, Imperial College London, London, UK

ABSTRACT: The development of floating offshore wind turbines (FOWTs) requires innovative anchoring systems capable of withstanding complex loading conditions. Conventional solutions, such as plate or pile anchors, often face limitations related to their installation and limited pullout capacity. This study introduces the root-inspired hybrid seabed anchor (HSA), a new expandable anchor inspired by plant roots, designed to provide high pullout capacity with a relatively simple installation process based on axial displacement. A series of reduced-scale experimental tests were conducted to (i) evaluate the effect of the number of anchor branches and the installation method on the response of HSAs, and (ii) characterize their performance under inclined loads for two soil densities. Results show that HSAs achieve pullout capacities up to 3 times higher than comparable piles under tensile loads. Inclined pullout resistance (tested for a loading angle of $\theta = 30°$) increases with the number of anchor branches (n_b), plateauing for $n_b > 4$ as the failure mechanism approaches that of a plate anchor. Installed anchors show significantly higher capacities than wished-in-place anchors (29% to 81% increase), highlighting the need to quantify installation effects to accurately predict anchor capacity. Soil density (from medium-dense to dense) increases anchor capacity by ~30%, but also increases the force needed to fully expand the anchor during installation. Interaction diagrams (*V-H* envelopes) for load inclination angles between 30° and 90° are well-captured by elliptical curves, showing a slight increase in capacity with inclination angle (from horizontal). These results support the potential of HSA as an efficient alternative for deep-water offshore wind turbines, combining a simple installation method and the ability to sustain inclined loads.

KEYWORDS: Root-inspired anchor, installation, pullout capacity, inclined loading.

1 INTRODUCTION

Floating wind represents 80% of the global wind energy potential (Global Wind Energy Council, 2023). A key challenge in the installation of floating offshore wind turbines (FOWTs) is the high cost and relatively low capacity of their foundations, which has motivated the development of new anchorage systems with high installation efficiency and load capacity.

Bio-inspiration, i.e., the adaptation of biological strategies to solve engineering problems, is a powerful tool for the development of novel technologies (Martinez et al., 2022). Tree root systems have evolved to maximize their capacity to mass ratio under the complex loading conditions induced by environmental loads. This similarity with the loading conditions experienced by civil infrastructure has motivated the study of the vertical (e.g. Burrall et al., 2020) and lateral loading resistance (e.g. Coutts, 1983) of tree roots, and the development of root-inspired foundations and anchors (e.g. Dyson et al., 2014, Dattola et al., 2020, Mallett et al., 2021, Houette et al., 2024). Still, most of the existing literature on root-inspired anchors/foundations has focused on the capacity of wished-in-place anchors, while the understanding of the effects of geometry, installation, and performance under inclined loads remains incomplete.

In this contribution we present the new root-inspired hybrid seabed anchor (HSA). The HSA is designed for easy installation, and high pullout resistance to the inclined loads encountered in offshore environments. Reduced-scale model tests were conducted to evaluate the effects of installation, geometry, soil density, and load inclination in the pullout response of HSA.

2 HYBRID SEABED ANCHOR (HSA)

The HSA is comprised by a vertical section and several laterally spread anchor branches mimicking the taproot and lateral roots (respectively) observed in nature (see Figure 1). The HSA consists of two components, a central shaft and a branched expandable anchor. The central shaft uses a standard 60° cone connected to a threaded rod and is used to aid penetration and guide the expanding anchor during installation. The branched expandable anchor is a cylindrical tube with slits along its axis placed over the cone's shaft. A groove carved around the outside of the anchor facilitates the bending of the anchor branches during installation.

2.1 *Installation method of HSA*

The installation of HSA follows a stage of vertical penetration into the soil, followed by an expansion stage with lateral branches spreading radially from the central shaft.

During initial penetration (Figure 1a-1b), the shaft and branched expandable anchor move downwards to a predetermined depth (d_e in 1d) with no relative movement between them. Next, during expansion, the central shaft is fixed in position, whilst the branched expandable anchor is pushed downwards (Figure 1b-1c). As the inner face of the branches enter contact with the shaft's cone, the branches are pushed outwards into the soil.

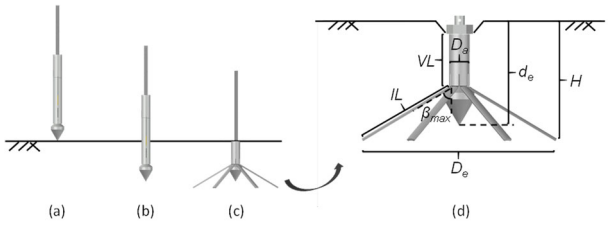

Figure 1. Schematic of a fully expanded HSA model: (a) Initial configuration prior to installation, (b) penetration stage, (c) expansion process, (d) geometry description.

2.2 *HSA geometry: branch length and angle*

The design of HSA follows the geometry proposed by Patino-Ramirez & O'Sullivan (2023). In their study, 2D discrete element analyses were carried out to find the optimal branch

inclination angle (β), and ratio between taproot (i.e. vertical length, VL) and branch (i.e. inclined length, IL) portions of the anchor, to maximize the vertical pullout capacity for a fixed anchor length. From their results, a ratio of branch to vertical length, IL/VL = 2 and a branch angle, β = 60° (adjusted from their reported value of 62° for ease of manufacturing) were adopted in this study. Figure 1 shows a schematic of the installation process (a-c) and the dimensions of the installed HSA (d), while the relevant dimensions of the HSA models are listed in Table 1.

Table 1. Geometry of HSA model.

Parameter	Symbol	Value	Unit
Anchor diameter	D_a	16	mm
Vertical length	VL	40	mm
Branch length	IL	80	mm
Maximum branch angle	β_{max}	60	°
Maximum expanded diameter	$D_{e,\,max}$	154	mm
Embedded depth	d_e	80	mm

The anchors were fabricated using aluminum tubes with a wall thickness of 1.6mm. Slits were machined along the tube's length to create the desired number of branches. A groove was machined around the anchor's circumference to separate the vertical and branch sections, and to facilitate branch bending during expansion. The anchor models are shown in Figure 2.

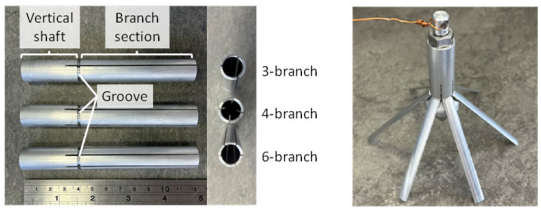

Figure 2. Prototype of HSA model. (a) Branched expandable anchor models before expansion, (b) Expanded HSA models.

3 EXPERIMENTAL SETUP

3.1 *Sample Preparation*

Model tests were conducted in a testing chamber with internal dimensions of 495 × 338× 300 mm (length × width × height) filled with dry Fuse sand 80/20. The sand has a median particle size of d_{50} = 0.50mm with coefficient of uniformity C_u = 1.29 and curvature C_c = 0.97. The maximum and minimum densities were reported as ρ_{max} = 1721 kg/m^3 and ρ_{min} = 1448 kg/m^3 respectively by Liu (2024).

Testing samples were prepared using air pluviation to a depth of 280 mm. The moving pluviation system follows the design of Gade & Dasaka (2017) and Patino-Ramirez et al. (2025), and is comprised of a cylindrical pluviator with 5 perforated acrylic diffuser plates, as shown in Figure 3a. During sample preparation, the pluviator was moved following a rectangular wave pattern; a vertical rod attached to the base of the pluviator was used to control the fall height, following the approach proposed by Fretti et al. (1995).

The relationship between pluviation fall height and relative density was established through a series of tests using a modified Proctor mold for fall heights between 0 and 40cm, as shown in Figure 3b. Two fall heights and target relative densities: 45% (h_f = 10cm) and 70% (h_f = 35cm) were selected for testing; and referred to as medium-dense and dense sand conditions herein (respectively). Boxplots in Figure 3b show the range of soil densities measured in this study.

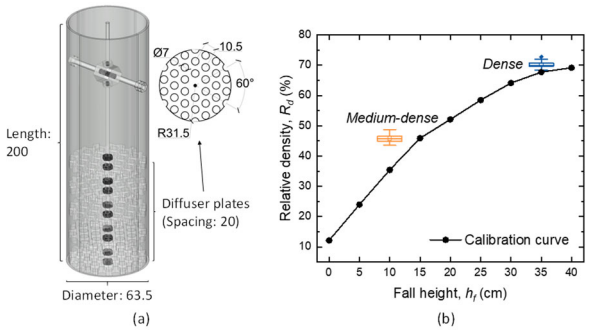

Figure 3. Sample preparation. (a) Moving pluviator design including outer cylinder and diffuser plates (dimensions in mm), (b) pluviation curve and boxplots showing the distribution of measured densities in medium-dense and dense samples. Enclosed box represents the inter-quartile range of the data, the centerline marks the median, and the whiskers extend to minimum and maximum values.

3.2 *Anchor installation setup*

Figure 4 illustrates the test setup for the installation of HSA (Mi, 2024). The testing chamber was placed on the base plate of a load frame and the HSA shaft was connected to a load cell mounted on the load frame's crossbeam. A metal loading beam was placed on top of the branched expandable anchor as a platform to place weights during anchor expansion.

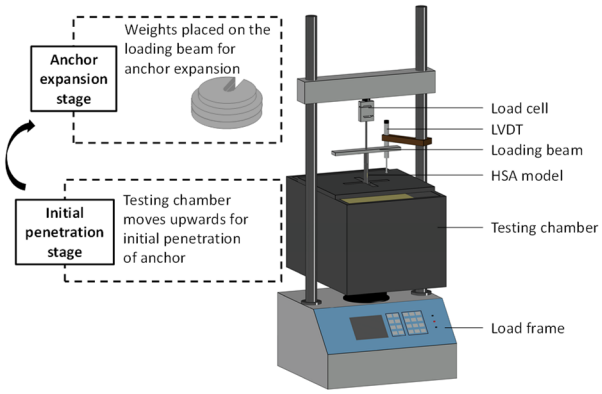

Figure 4. Schematic of anchor installation setup and procedure.

During the initial penetration stage, the central shaft and branched anchor remained in place, whilst the testing chamber moved upwards at 10mm/min until the tip of the cone reached the desired depth of embedment, d_e (see Figure 1b). The penetration resistance as a function of displacement was measured with the load cell and linear displacement transducer (LVDT) shown in Figure 4.

Next, during the expansion stage, weights were sequentially placed on the loading beam to induce anchor expansion. Spatial constraints of the setup limited the maximum expansion force to 700N, which prevented complete expansion of the anchors. To account for this limitation, the anchor's expanded diameter was measured after testing, ranging from 106mm to 150mm for different number of anchor branches and soil densities. Further details on installation results are shown in section 4.2.

3.3 *Pullout setup*

After anchor installation, the central shaft and loading beam were removed and a nut and a hook (pad-eye) were screwed onto the top of the anchor (Figure 2b). The nut prevented backsliding of the anchor branches during and after pullout. A copper wire (mooring line) was attached to the pad-eye and threaded around an adjustable pulley system mounted on the testing chamber (see Figure 5), before reaching the load cell at

the load frame's crossbeam (see Figure 4). The load inclination angle θ (measured from the horizontal plane) ranged between 30° and 90°, and was set by adjusting the lateral position of the lower pulley. Pullout was achieved by lowering testing chamber at a rate of 5mm/min, and the pullout force and displacement were measured using the same load cell and LVDT used during installation.

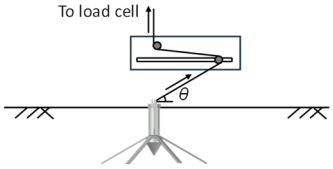

Figure 5. Schematic of pullout test setup.

4 EFFECT OF NUMBER OF BRANCHES AND INSTALLATION

4.1 *Number of anchor branches*

Previous studies have showed that the number of anchor branches (n_b) has a significant influence on pullout stiffness and capacity of root-inspired anchors (Mallett, 2019; Miller, 2021). Experimental results from Mallett (2019) using a similar simplified root-inspired anchor showed that the increase in vertical pullout capacity with increasing number of branches (n_b) plateaus for $n_b > 6$. We expand these observations for inclined loading ($\theta = 30°$, medium-dense sand) for anchors with $n_b = 3$, 4 and 6. In addition, an unexpanded anchor i.e., a pile with the same total length as the anchors, referred to as $n_b = 0$, was included as a benchmark for comparison. The load-displacement curves for HSA models with different numbers of branches are shown in Figure 6; all tests were carried out in medium-dense sand at a load inclination $\theta = 30°$.

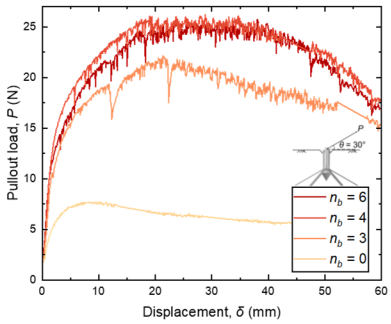

Figure 6. Load-displacement curves for HSA with 0, 3, 4 and 6 branches in medium-dense sand pulled out at $\theta = 30°$.

A significant increase in pullout capacity was observed with number of branches, with the 6-branch HSA having a peak load over 3 times of that of the pile anchor ($n_b = 0$). To account for the differences in expanded diameter across anchors (ranging from 106mm to 150mm for these experiments), the pullout force (P) and displacement (δ) were normalized. The displacement was normalized by expanded anchor diameter (δ/D_e), while the pullout capacity was reported in terms of the anchor capacity factor or breakout factor, N_γ (Merifield & Sloan, 2006, Mallett, 2019), calculated as:

$$N_\gamma = \frac{4P}{\pi\gamma' D_e^2 H'} \quad (1)$$

where D_e is the expanded diameter of the anchor (Figure 1), γ' is the effective unit weight of soil. H' represents the equivalent height of a cylinder with the same volume as the soil above the anchor, calculated as:

$$H' = H - \frac{IL\cos\beta}{3} \quad (2)$$

Figure 7 shows the normalized pullout responses for n_b = 3, 4 and 6, as N_γ is not well-defined for n_b = 0. A significant 60% increase in N_γ was observed between the 3- and 4-branch models, whereas the 6-branch HSA only showed a slight increase of 7% versus the 4-branch model. The increase in N_γ with n_b can be attributed to the soil arching between adjacent branches. This observation is supported by the digital volume correlation (DVC) results from Mallett (2019), who observed that the height of soil arch was significantly lower for n_b = 6 than n_b = 3 in vertical pullout tests.

We hypothesize that a similar mechanism occurs under inclined loading, with soil arching also contributing to the observed rotational resistance during inclined loading of HSA. Further, the diminishing increase in N_γ for $n_b > 4$ suggests that the developed soil arch approaches a minimum height, resembling the mobilization mechanism of plate anchors.

Subsequent pullout tests focused exclusively on the 6-branch HSA across a range of loading conditions.

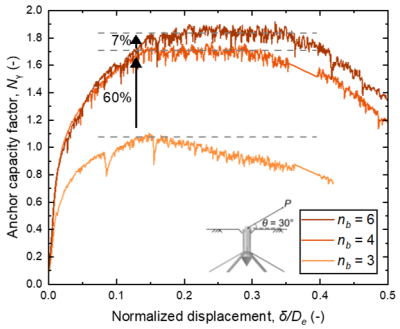

Figure 7. Normalized load-displacement curves for HSA with 3, 4 and 6 anchor branches in medium-dense sand, at a load inclination $\theta = 30°$.

4.2 *Insights of HSA installation*

Figure 8 shows representative curves of penetration resistance during the first stage of installation. After an initial stage of low penetration resistance (first ~10mm) the resistance increased near-linearly with displacement for both relative densities. Tests in dense sand exhibited greater penetration resistance compared to those in medium-dense sand. By the end of anchor penetration, the resistance in dense sands reached 33N, which was 37% higher than the 24N observed in medium-dense sand. Differences across tests with the same pluviation fall height were attributed to variability in soil density as reported in Figure 3b.

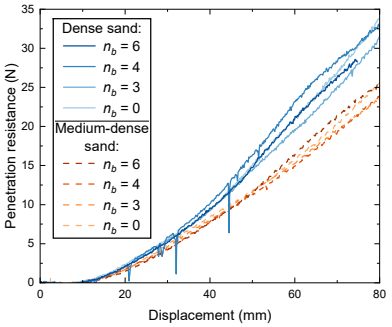

Figure 8. Penetration resistance during initial penetration stage.

Next, the anchor expansion stage was carried out using dead weights to the same maximum expansion force for all tested conditions. The resulting expanded diameters (measured

after pullout) for different soil densities and numbers of branches are shown in Figure 9. At the low levels of stress in the experiments, no significant bending of the anchor's branches is expected, therefore, the post-excavation values of expanded diameter are considered representative of the conditions during pull-out.

The achieved expanded diameter was maximum for $n_b = 3$ in medium-sand and decreased with increasing sand density and a higher number of branches. The number of branches had the highest influence, reducing by 20% (medium-dense) and 26% (dense) the expanded diameters from $n_b = 3$ to 6. Increasing sand density also reduced the expanded diameter of the anchors by 12% (in average) for anchors with $n_b = 6$.

We attribute the increase in expansion resistance to the larger projected normal area between soil and expanding branches with increasing n_b. For instance, for $n_b = 3$ the projected width of each branch corresponds to $\frac{\sqrt{3}}{2} D_a$ (side of the equilateral triangle inscribed in the body of the anchor), while the same for $n_b = 6$ is equal to $\frac{D_a}{2}$. As a result, $n_b = 6$ has a total projected area ~16% larger than that of $n_b = 3$, engaging a larger volume of soil and passive resistance. Further, the increase in expansion resistance with density can be attributed to the increased shear strength of the material, affecting the passive response of the soil.

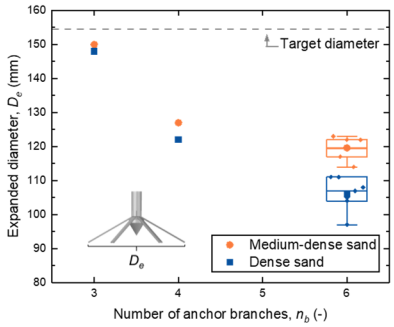

Figure 9. Expanded diameter after anchor expansion measured after pullout. Scattered points correspond to the average expanded diameters for each scenario, and boxplots show the variability of the measurements for the 12 6-branch HSAs tested in the experiments.

4.3 *Effect of installation on pullout resistance*

A series of pullout tests were also carried out on wished-in-place HSA models to investigate the effect of installation in their pullout response. The comparison focused on the performance of 6-branch HSAs in dense sand for 5 different load inclinations (between 30° and 90°). Wished-in-place anchors had an expanded diameter D_e = 120mm, while the average D_e across installed models was 106mm (see corresponding boxplot in Figure 9).

Figure 10a shows a representative comparison between the load-displacement response of wished-in-place and installed HSAs for a loading angle $\theta = 60°$. Generally, installed anchors exhibited higher normalized anchor capacity, mobilized at a smaller displacement. For loading angles $\theta \geq 60°$, the normalized displacement to peak resistance was 17% lower for installed anchors versus wished-in-place anchors.

Figure 10b shows the interaction diagrams for wished-in-place and installed HSAs. Interaction diagrams are built using the horizontal ($N_{\gamma h}$) and vertical ($N_{\gamma v}$) components of the peak anchor capacity factors (N_γ) from the load-displacement plot. The pullout capacity of installed anchors was significantly higher than that of wished-in-place anchors, with increases ranging between 29% ($\theta = 30°$) and 81% ($\theta = 90°$).

These differences in capacity may be explained by non-homogeneities and zones of low sand density around the wished-in-place anchors during dry pluviation. Hao et al. (2019) and Schiavon et al. (2020) observed similar effects during wished-in-place testing of helical piles, claiming that 'umbrella' or 'shadowing effects' during air pluviation may lead to regions of lower density around wished-in-place structures.

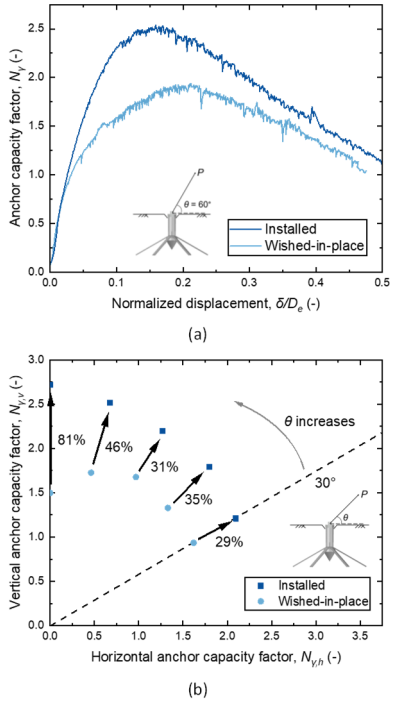

Figure 10. Comparison of pullout performance between wished-in-place and installed 6-branch HSA models in dense sand: (a) representative load-displacement response (θ = 60°), (b) interaction diagram for pullout angles between 30° and 90°.

In contrast, installed anchors avoid non-uniformities during sample preparation, and the process of anchor penetration and expansion may also induce local soil densification. Local soil densification increases soil stiffness and shear strength within the anchor's zone of influence, which may explain the higher pullout capacity and stiffer response observed during pullout.

The interaction diagram in Figure 10b shows a reduction in the relative difference between N_γ of installed and wished-in-place anchors, as the load deviated from the vertical direction (θ = 90°). This observation may suggest that the zone of disturbance around wished-in-place anchors is limited to the concentric region around the anchor, affecting the response to vertical or moderately inclined loading (θ = 60° to 90° in this study), but becoming less prevalent for inclined loads, where the failure mechanism extends beyond the zone of disturbance. Further testing and micro-mechanical observations are needed to confirm or refute these hypotheses.

5 PERFORMANCE UNDER INCLINED LOADING

5.1 *Load-displacement responses*

Pullout tests were conducted on fully installed (as opposed to wished-in-place), 6-branch HSA models under 5 different inclination angles, from $\theta = 30°$ to $\theta = 90°$ (vertical). The load-displacement curves are shown in Figure 11a. The results showed an increase in secant stiffness to peak load with inclination angle, consistent with findings by Roy et al. (2022) for plate anchors and Huang et al. (2020) for pile anchors.

At lower inclination angles (θ = 30° in this study), the response appeared more ductile, with peak loads mobilized at large displacements (exceeding 0.4D_e) and sustained over broader displacement ranges, resembling the response of rigid piles under lateral and moment loading. Murff and Hamilton (1993) described such mechanisms analytically, assuming a soil wedge that deforms and slips along a shear failure surface while the pile (or HSA in this case) rotates and translates, inducing soil flow below the wedge. The presence of anchor branches is expected to enlarge the volume of the mobilized soil wedge at failure, while similar horizontal soil flow patterns develop around the anchor's body.

The observed surface deformation at the end of the test (Figure 11b) may be explained by the mobilization of this soil wedge, which induces surface heaving in the direction of loading. This mechanism facilitates anchor rotation during pullout, allowing the anchor to sustain higher N_γ over a larger displacement range.

For higher inclination angles (θ = 60°, 75°, and 90°), the load-displacement response exhibited a distinctive brittle behavior, reaching peak capacity at smaller displacements (0.1–0.15D_e) followed by a rapid loss in resistance with relatively small post-peak displacement. This behavior was consistent with previous studies on the vertical pullout of root-inspired anchors (e.g. Kim et al., 2024; Houette et al., 2024), indicating the dominance of vertical (translational) failure mechanism, where the surface soil wedge primarily slipped along the failure surface with minimal soil flow beneath (Figure 11b).

In tests for θ = 45°, the peak was mobilized at around 0.3D_e in dense sand and 0.2D_e in medium-dense sand, before a sudden reduction in resistance occurred. This behavior suggests the existence of a transitional mechanism, from a mechanism controlled by horizontal soil flow, to one controlled by vertical translational failure.

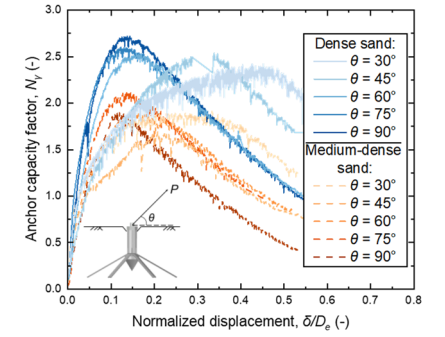

(a)

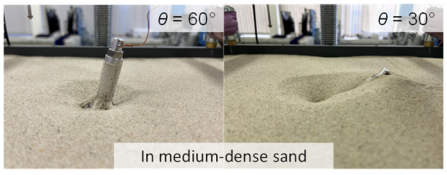

(b)

Figure 11. Effect of pullout inclination angle for installed 6-branch HSA models: (a) normalized load-displacement responses in both dense sand (solid lines) and medium-dense sand (dashed lines), (b) End-of-test HSA model positions captured for tests in medium-dense sand.

5.2 *Failure envelopes for inclined loading*

Figure 12 shows the interaction diagrams for inclined pullout resistance of HSA for the two soil densities tested. For each density, 5 tests with inclination angles ranging from 30°-90° were performed, and the N_γ at peak split into vertical and horizontal components. Interaction diagrams were well captured by elliptical curves centered at the origin. The shape of the interaction diagrams was similar across densities, with an aspect ratio of ~1.13 ($N_{\gamma v,max}/N_{\gamma h,max}$) for both dense ($R^2$ = 0.998) and medium-dense conditions (R^2 = 0.972).

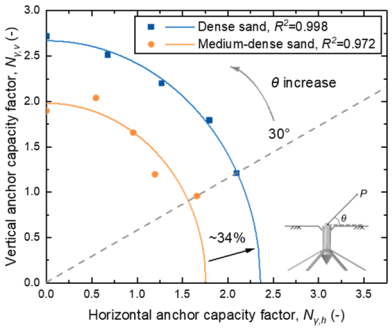

Figure 12. Interaction diagrams for installed 6-branch HSA models. Discrete points correspond to the test data and curves correspond to the fitted elliptical envelopes centered at the origin.

A significant increase in anchor capacity (~34%) was observed between dense and medium-dense conditions. The aspect ratio of the envelopes showed only a slight reduction (8.6%) in capacity at θ = 30° versus θ = 90°. However, the observed anchor rotation during pullout (Figure 10b) suggests that ultimate capacity involved not only translational components ($N_{\gamma h}$ and $N_{\gamma v}$) in the interaction diagrams (Figure 12), but also mobilization of moment resistance. Due to physical limitations of the model tests, the rotation center and the exact inclination angle at peak capacity could not be accurately identified. As a result, moment capacity could not be quantitatively resolved.

Variations in embedment depth, pad-eye location, and anchor geometry are expected to influence moment resistance and failure mechanisms, resulting in different paths within the three-dimensional (*V–H–M*) failure envelope (Gottardi & Butterfield, 1993; Martin, 1994). Further studies are needed to systematically explore these effects on HSA performance under inclined and moment loading.

6 CONCLUSIONS

Reduced scale physical model tests were conducted to test the installation and pullout response of the Hybrid Seabed Anchors (HSA), focusing on the effect of anchor geometry (in terms of the number of anchor branches), installation effects, soil density and loading inclination angle on the pullout response of HSA.

The main findings of this study are:

- The number of anchor branches significantly affects HSA pullout capacity under inclined loading. At θ = 30°, a 60% increase in capacity was observed from 3 to 4 branches, followed by a 7% increase from 4 to 6 branches. The plateauing increase in capacity for n_b > 4 is explained by arching between branches, which leads to a failure mechanism resembling that of plate anchors.
- Installed HSA models showed higher capacity than wished-in-place models, with larger differences observed for higher angles (closer to the vertical). This is attributed to induced lack of soil uniformity around the wished-in-place anchors during sample preparation, as well as to local soil densification during installation. These observations highlight the importance of quantifying installation effects in the design of anchoring systems.
- Tests in medium-dense and dense sand revealed that the increase in shear strength and passive resistance associated with higher soil density leads to higher penetration forces, limits the expansion of the anchor during installation, whilst also increasing the anchor's pullout capacity.

- Testing at load inclinations between 30° to 90° revealed a transition between failure mechanisms. At angles above 60° the response is brittle and the failure is dominated by the translational movement of the soil wedge around the anchor. In contrast, for loading angles below 45°, the response is ductile and the failure mechanism is governed by the deformation of the lateral soil wedge accompanied by a flow mechanism beneath the failure surface.
- The *V-H* interaction diagrams for the 6-branch HSA were well captured by elliptical envelopes ($R^2 > 0.97$). The envelopes' aspect ratio ($N_{\gamma v,max}/N_{\gamma h,max}$) was similar across sand densities (1.13), with anchors in dense sand yielding a ~34% larger envelope. The interaction diagrams reveal the ability of HSA to sustain inclined loads, with an 8.6% reduction in N_γ at $\theta = 30°$ compared to $\theta = 90°$ (vertical).

This study assesses the suitability of the HSA as a foundation system for offshore conditions. The results show significant differences between the behavior of wished-in-place vs. installed anchors, highlighting the importance of installation effects. The installation method of HSA is proposed to overcome the prevailing installation limitations of plate and root-inspired anchors. Yet, the significantly large forces needed for expansion prevented full expansion of the anchors in this study, and remain a challenge in the large-scale adoption of HSA. Future work will focus on refining the design of HSA to simultaneously improve the installation efficiency and the pullout resistance of HSA.

The results presented support the potential of HSA as a feasible anchoring method; still, the interpretation of these results must consider the inherent limitations of reduced-scale model tests, which require validation at their representative scales. For instance, smaller effects of dilation are expected at the stress levels encountered in the field, which may result in less evident effects of local densification during installation. Similarly, reduced arching at large-scale may lead to different relations between number of anchor branches and pullout capacity. Future work may also benefit from micro-mechanical observations. These studies can provide insight into the underlying failure mechanisms and support the development of analytical models for predicting resistance. Additionally, the effects of pad-eye location and embedment depth on pullout performance should be explored using more comprehensive instrumentation, enabling the development of a full failure envelope in the *V–H–M* space.

7 ACKNOWLEDGEMENTS

The experimental campaign presented was carried out at Geotechnics Laboratory at Imperial College London. The authors would like to acknowledge the support of the laboratory staff. Supervision and help from Dr. Rowena Stevenson is also greatly acknowledged.

8 REFERENCES

Burrall, M., DeJong, J. T., Martinez, A., and Wilson, D. W. 2020. Vertical pullout tests of orchard trees for bio-inspired engineering of anchorage and foundation systems. *Bioinspiration & Biomimetics*, 16(1), 016009.

Coutts, M.P. 1983. Root architecture and tree stability. *Plant and soil*, *71*(1), 171-188.

Dattola, G., Ciantia, M., Galli, A., Blyth, L., Zhang, X., Knappet, J., Castellanza, R., Sala, C., and Leung, A. 2020. A macroelement approach for the stability assessment of trees. *Proc. CNRIG 2019: Geotechnical Research for Land Protection and Development*, Lecco, 417–426.

Dyson, A. and Rognon, P. 2014. Pull-out capacity of tree root inspired anchors in shallow granular soils. *Geotechnique Letters*, 4(4), 301–305.

Fretti, C., Lo Presti, D.C.F. and Pedroni, S. 1995. A pluvial deposition method to reconstitute well-graded sand specimens. *Geotechnical testing journal*, 18(2), 292-298.

Gade, V.K. and Dasaka, S.M. 2017. Assessment of air pluviation using stationary and movable pluviators. *Journal of Materials in Civil Engineering*, 29(5), 06016023.

Global Wind Energy Council, 2023. *Global offshore wind report 2023*. Brussels, Belgium.

Gottardi, G. and Butterfield, R.O.Y. 1993. On the bearing capacity of surface footings on sand under general planar loads. *Soils and foundations*, 33(3), 68-79.

Hao, D., Wang, D., O'Loughlin, C.D. and Gaudin, C. 2019. Tensile monotonic capacity of helical anchors in sand: interaction between helices. *Canadian Geotechnical Journal*, 56(10), 1534-1543.

Houette, T., Dibia, M., Mahabadi, N., and King, H. 2024. Pullout resistance of biomimetic root-inspired foundation systems. *Acta Geotechnica*, 19(3), 1191–1210.

Huang, T., O'Loughlin, C., Gaudin, C., Tian, Y. and Lu, T. 2020. Drained response of rigid piles in sand under an inclined tensile load. *Géotechnique Letters*, 10(1), 30-37.

Kim, Y.A., Burrall, M., Jeon, M.K., DeJong, J.T., Martinez, A. and Kwon, T.H., 2024. Pullout behavior of tree root-inspired anchors: development of root architecture models and centrifuge tests. *Acta Geotechnica*, 19(3), 1211-1229.

Liu, S. 2024. *Predicting the min/max density of granular materials from their shape and size distributions*. Master's Dissertation, Imperial College London.

Mallett, S. D. 2019. *Mechanical behavior of fibrous root-inspired anchorage systems*. Ph.D. Thesis, Georgia Institute of Technology.

Mallett, S. D., Frost, J. D., and Huntoon, J. A. 2021. Root-inspired anchorage systems for uplift and lateral force resistance. *Proc. International Foundations Congress and Equipment Expo 2021*, Dallas, 299–307.

Martin, C. 1994. *Physical and numerical modelling of offshore foundations under combined loads*. Ph.D. Thesis, Oxford University.

Martinez, A., DeJong, J., Akin, I., Aleali, A., Arson, C., Atkinson, J., Bandini, P., Baser, T., Borela, R., Boulanger, R., et al. 2022. Bio-inspired geotechnical engineering: principles, current work, opportunities and challenges. *Géotechnique*, 72(8), 687–705.

Merifield, R.S. and Sloan, S.W. 2006. The ultimate pullout capacity of anchors in frictional soils. *Canadian geotechnical journal*, *43*(8), 852-868.

Mi, Y. 2024. *Experimental testing of Hybrid Seabed Anchors (HSA) under inclined loading*. Master's Dissertation, Imperial College London.

Miller, J. V. 2021. *Multi-directional loading of 3d-printed tree root models using a six-axis robotic arm*. Master's Dissertation, University of California, Davis.

Murff, J.D. and Hamilton, J.M. 1993. P-ultimate for undrained analysis of laterally loaded piles. *Journal of Geotechnical Engineering*, 119(1), 91-107.

Patino-Ramirez, F. and O'Sullivan, C. 2023. 'Pull-out resistance of root-inspired anchors under combined loading.' *Engineering Mechanics Institute Conference*, Atlanta, USA, 6-9 June.

Patino-Ramirez, F., Yang, Y., Salomon, J., Holmes, A.S. and O'Sullivan, C. 2025. Horizontal Penetration in Granular Media: Effect of Intruder Shape, Depth, Orientation, and Material Density on Penetration Forces. *Journal of Geotechnical and Geoenvironmental Engineering*, 151(7), 04025063.

Roy, A., O'loughlin, C.D., Chow, S.H. and Randolph, M.F. 2022. Inclined loading of horizontal plate anchors in sand. *Géotechnique*, 72(12), 1051-1067.

Schiavon, J.A., Tsuha, C.D.H.C. and Thorel, L. 2020. Study on the installation effect of helical piles in very dense sand. *Proc. 4th European Conference on Physical Modelling in Geotechnics*, Luleå, 151-156.